

Features of the shape of the emission spectrum of a spherical microresonator with a high refractive index luminescent shell due to the polarization of the whispering gallery modes

© A.A. Dukin, V.G. Golubev

Ioffe Institute, St. Petersburg, Russia

e-mail: dookin@gvg.ioffe.ru

Received 2022

Revised 2022

Accepted 2022

The effect of the thickness and refractive index of the shell on the amplitudes of lines of the TE and TM polarized whispering gallery modes (WGMs) in the emission spectrum of a microcavity structure consisting of a spherical core covered with a luminescent shell with a refractive index greater than that of the core is studied. The luminescence spectra of the shell, the radial distribution of the WGM field, and the mode parameters (wavelength, quality factor, and effective volume) are calculated using the method of spherical wave transfer matrices. It is shown that at certain subwavelength shell thicknesses, the amplitude of the TE mode emission peak is many times greater than the amplitude of the TM mode peak with the same polar, azimuthal, and radial indices. This is explained by the fact that with these parameters of the shell, WGMs propagate inside the shell as waveguide modes.

Keywords: spherical microresonator, high refractive index luminescent shell, whispering gallery modes, mode polarization, amplitude of emission lines.

DOI: 10.21883/EOS.2022.11.55107.3857-22

Introduction

Spherical microresonators (MR) possess unique optical properties that make them drawing a great attention in different areas of optics [1–7]. Their properties are based on whispering gallery modes (WGM) i.e. eigenmodes of the electromagnetic field of spherical microresonator. The WGMs are characterized by high Q-factor in a wide range of wavelengths and low effective volume of photon mode localization. WGMs have two types of polarization: TE, when the electric field vector is parallel to the MR surface, and TM, when the electric field vector is normal to the MR surface. The WGM field inside a MR propagates as a travelling wave, which experiences a total internal reflection from the interface with the environment. Beyond the external boundary there is an area of exponentially decaying evanescent field.

An important field of application for microspheres with WGMs is the sensorics. Microspheres can be used for detecting refractive index of the environment, chemical substances, biological substances, pressure, temperature [1,5,8–11]. Adsorption of molecules or particles on the MR surface or a change in the refractive index of the environment result in a change in the refractive index in the local area near the MR surface, where the evanescent field of WGM is localized, which causes a change in the WGM wavelength. Sensitivity of sensors can be improved due to the use of core-shell type structures, where a central optically transparent MR core is coated by a concentric spherical shell with a refractive index greater than that of the core [12–14]. Electromagnetic field of the WGM is

concentrated in this shell, which increases the evanescent field amplitude, that, in turn, induces a greater polarization in the environment or in the adsorbate, thus improving the sensor's sensitivity.

Passive MRs used as sensors require high-precision interfacing with signal input-output devices, such as optical waveguides, prisms, etc., which limits their application. Active MRs that contain luminescent materials, have no this limitation, because the optical signal is excited and detected remotely. The luminescent shell can be made of light-emitting materials, for example, such as semiconductors [15], silica doped with rare-earth metal ions [16]. Nanoporous material can be used as a shell (for example, nanoporous silica [17–19]), provided that the greater portion of pore volume will be filled with light-emitting materials with high refractive indices. The introduction of wide-band emitters into MRs allows for simultaneous recording of a set of narrow luminescence lines corresponding to WGMs, and this can be used to increase the sensitivity of biological substances detection [20,21].

An increase in the luminescent sensors sensitivity can be achieved through the use of small-diameter microspheres — less than $10\ \mu\text{m}$ [20,21]. The sensor sensitivity (narrow line shift in the spectrum) is inversely proportional to the microsphere radius and increases with decrease in the radius, which forms the base for the benefit of using small-diameter microspheres (up to a few microns). An additional advantage of small-diameter microspheres is the lower density of the WGM frequency spectrum due to the fact, that only modes with radial index $q = 1$ remain

in the spectrum and the intermode interval between them increases. This facilitates the identification of modes, as well as detection and analysis of a group of WGM lines in one spectrum simultaneously [21]. In the case, when a small-diameter MR and its external luminescent shell are made of non-cytotoxic materials, such as, for example, nanoporous silica, the MR can be introduced directly into a living cell for a noninvasive research. Coating the MR surface with specific ligands ensures their targeted delivery to cells due to the ligand-receptor interaction. Thus, an opportunity opens for microscopic biological research activities *in vitro*.

The sensitivity of sensors based on the core-shell structures with greater refractive index of the shell is different for TE- and TM- modes [13], that's why taking into account the WGM polarization is important. The conditions for electric field on the interface between two media with different refractive indices are different for TE- and TM-polarized waves, and this results in that spherical waves with different polarizations have different coefficients and phases of reflection from the spherical boundary [22]. As a result, field of TE- and TM- polarized modes penetrates through the shell boundary in different manner and concentrates in the core and in the shell in different degrees [23]. Therefore, an effect of the WGM polarization on the amplitude of lines of the radiation from the luminescent shell can be expected.

The purpose of this study is to investigate the effect of refractive index and thickness of the luminescent shell on the amplitude of radiation lines that correspond to WGMs with different polarization. We have modeled the radiation spectrum of a MR-structure, composed of a small-diameter ($3.5\mu\text{m}$) spherical core covered with a luminescent shell (with a thickness of 10, 80, and 500 nm) with a refraction index greater than that of the core.

MR-structure under study and luminescence spectra modeling method

In this study we have analyzed spherical MRs of the core-shell type, where a luminescent shell with a refractive index greater than that of the core is applied on a spherical optically transparent dielectric core.

The shell radiates in WGMs. Modes are described by spherical waves, which are characterized by three numbers: polar index l ($l \geq 1$), azimuth index m ($m = l$ or m close to l), radial index q ($q \geq 1$) and two polarizations (TE and TM). The field with TE-polarization does not have radial component of the electric field, the field with TM-polarization does not have radial component of the magnetic field. In the text below WGMs are denoted as TE_l^q or TM_l^q , where TE and TM-are WGM polarizations, q and l are corresponding indices.

The spectra of shell radiation, the radial distribution of the field and WGM parameters (wavelength, Q-factor, polarization, polar and radial indices, effective volume of the mode) are calculated using the electromagnetic wave

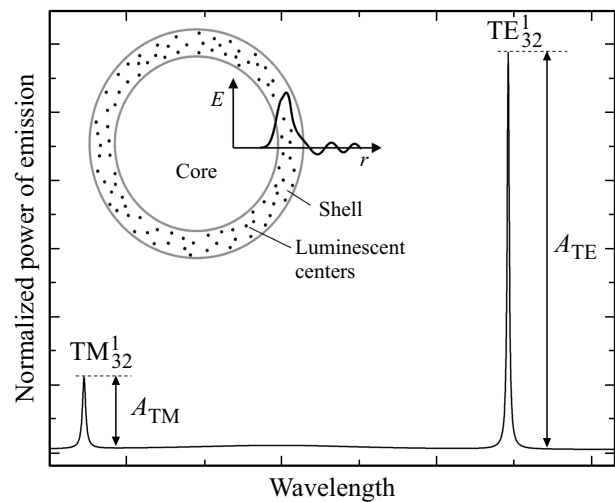


Figure 1. Typical spectral dependence of the radiation intensity of a luminescent shell surrounding a spherical core. Modes are indicated above peaks. Amplitude of peaks A_{TE} and A_{TM} is indicated near peaks. The insert schematically shows cross-section of the modeled structure, where two concentric circles show boundaries of the shell, and a graph is superimposed on them, showing typical distribution of the electric field strength (E) along the radial coordinate (r) for the TE-polarized WGM with $q = 1$. Dots indicate luminescent centers in the shell.

field expansion in the basis of vector spherical harmonics and the method of spherical wave transfer matrices [24]. Calculated profiles of the radial distribution of the field are normalized in such a way, that amplitude of the electric field strength at the maximum is 1. For more details of the calculation procedure please refer to [25].

We have investigated the spectra of shell radiation in a structure with the following parameters: core diameter $3.5\mu\text{m}$, refractive index of the core $n_{\text{co}} = 1.46$, refractive index of the shell n_s varying in the range of 1.46–2.25, thickness of the shell varying in the range of 10–500 nm. Magnetic permittivity of all media is equal to 1, no absorption. Diameter and refractive index of the core correspond to parameters of microspheres made of silica, that are produced by hydrolysis of tetraethoxysilane in the alcohol-water-ammonia medium [15]. The region of maximum values of n_s in the investigated range corresponds to refractive indices of semiconductor materials, for example, SiC ($n_s = 2.25$). The SiC shell is produced by the method of plasma-enhanced chemical vapor deposition described in [15]. The region of minimum and medium values of n_s corresponds to the refractive index of porous silica with its pores almost completely filled with light-emitting materials with refractive indices greater than 1.46.

The radiation spectrum of a luminescent shell is composed of pair of narrow peaks, that correspond to the radiation of WGMs with the same indices l and $q = 1$, but with different polarization TE and TM [24].

Fig. 1 shows a typical radiation spectrum of a spherical MR shell in a narrow range of wavelengths. The insert

shows schematic image of cross-section of the modeled structure illustrating the typical distribution of the electric field strength along the radial coordinate for the TE-polarized WGM with $q = 1$.

For our analysis we have used TE_{32}^1 and TM_{32}^1 modes with A_{TE} and A_{TM} amplitudes, respectively, which have their wavelengths at the defined MR parameters within the optical range of the spectrum. We have considered structures with a shell thickness of 10, 80, and 500 nm, that correspond to the cases, when its optical thickness is much less, comparable, or greater than wavelengths of these modes.

Results and discussion thereof

Fig. 2 shows the calculated distribution of squared modulus of electric field strength and distribution of normalized effective potential of TE_{32}^1 and TM_{32}^1 modes over the radial coordinate for three thicknesses of the shell (10 nm — (a, d), 80 nm — (b, e), 500 nm — (c, f)) with a refractive index of $n_s = 2.25$. In figures of field profiles (Fig. 2, a, b, c) vertical solid lines show boundaries between the shell and the core and the environment, in figures of the effective potential (Fig. 2, d, e, f) vertical lines show boundaries of the potential well and the potential barrier for the TE-mode (r_m^{TE} and r_b^{TE} — dashed lines) and the TM-mode (r_m^{TM} and r_b^{TM} — solid lines), as well as the boundary between the shell and the environment (r_s). The horizontal dash-dotted line at the level of 1 corresponds to the energy level in the effective potential.

The equation for radial dependence of the electric field of the mode corresponds to the Schrodinger equation for one-dimensional motion of particle in the effective potential:

$$V_{ef} = E \left([1 - n(r)^2] + \frac{l(l+1)}{r^2 k_0^2} \right),$$

where $n(r)$ is refractive index, depending on the radial coordinate, r is radial coordinate, k_0 is wave vector in vacuum ($k_0 = 2\pi/\lambda$), λ is wavelength of the mode in vacuum, l is polar index, $E = \hbar^2 k_0^2 / 2M = \hbar\omega$ is energy, $M = \hbar\omega / 2c^2$ is reduced mass [26]. This potential depends on the wavelength of the mode and, respectively, it is different for TE_{32}^1 and TM_{32}^1 modes. It is formed by the centrifugal potential (term $l(l+1)\lambda^2/r^2(2\pi)^2$) and the refractive index, that depends on the radial coordinate (term $[1 - n(r)^2]$). The effective potential has the form of classical potential well (Fig. 2, d), where photon moves between points of turn r_m and r_s (radius of the shell boundary with the environment). Thus, the WGMs are characterized by the fact that they are located in a potential well formed by the centrifugal potential from the side of core and the potential at the boundary with the environment, that undergoes a step change. In the region of $r_s < r < r_b$ there is a potential barrier of triangular shape. In the region of $r < r_m$ and in the region of barrier ($r_s < r < r_b$) the field of the mode decays exponentially, in the latter case it is the region of

the evanescent field. Width and Q-factor of the mode are determined by the probability of tunneling through this barrier. Since the effective potential depends on the squared wavelength of the mode, then all points of r_m and r_b , as well as width and height of this potential barrier are different for TE- and TM- modes. The presence of a shell with refractive index greater than the refractive index of the core results in formation of an additional potential well formed by the step changes of the refractive index at boundaries of the shell (the dip on the graph of the effective potential in Fig. 2, d, e, f).

The selected thicknesses correspond to three different cases of radial distribution of field of the investigated modes in the shell. For the TE-mode graphs of the radial distribution of the field are continuous curves with one wide maximum. For the TM-mode there are two step changes on the graphs at the shell boundaries, which arise due to the boundary conditions for the radial component of the electric field at the interface between two media with different dielectric permittivity values.

With a shell thickness of 10 nm (Fig. 2, a) the region of field localization of both modes along the radial coordinate is much larger than its thickness, and the major portion of radial distribution of the field of both modes and its maximum are in the core. In the region of shell there is a minor portion of the field profile of TE-mode in the region of distribution decay. For the profile of TM-mode there is a deep dip in the region of the shell. With this thickness (Fig. 2, d) both modes are limited by the centrifugal potential in the region of core and the potential at the interface with the environment, that undergoes a step change, and, thus, both modes propagate as WGM in the core. At the same time wavelengths of TE- and TM- modes are close to each other, so the potential barriers for them are insignificantly different (Fig. 2, d), and, as a consequence, Q-factors of the modes are close to each other (Fig. 3, a).

With a thickness of 500 nm the region of localization for both modes is comparable with the shell thickness and almost completely resides in the shell (Fig. 2, c). Since the electric field strength on the inner boundary of the shell is low, the reflection on it has a little effect on the modes. It can be considered that the structure in question corresponds to a uniform sphere with a refractive index equal to n_s , where the outer layer of the sphere is radiative, having its thickness equal to the shell thickness. With a thickness of 500 nm (Fig. 2, f) both modes are limited by the centrifugal potential inside the shell and the potential at the interface with the environment, that undergoes a step change, and, thus, both modes propagate as WGM within the shell. At the same time wavelengths of TE- and TM- modes are close to each other, so the potential barriers for them are (Fig. 2, f), and, as a consequence, Q-factors of the modes (Fig. 3, c) differ insignificantly from each other.

The case of thickness equal to 80 nm (Fig. 2, b) is an intermediate, that is the field is localized in both the region of shell and in the core, with the reflection on the inner

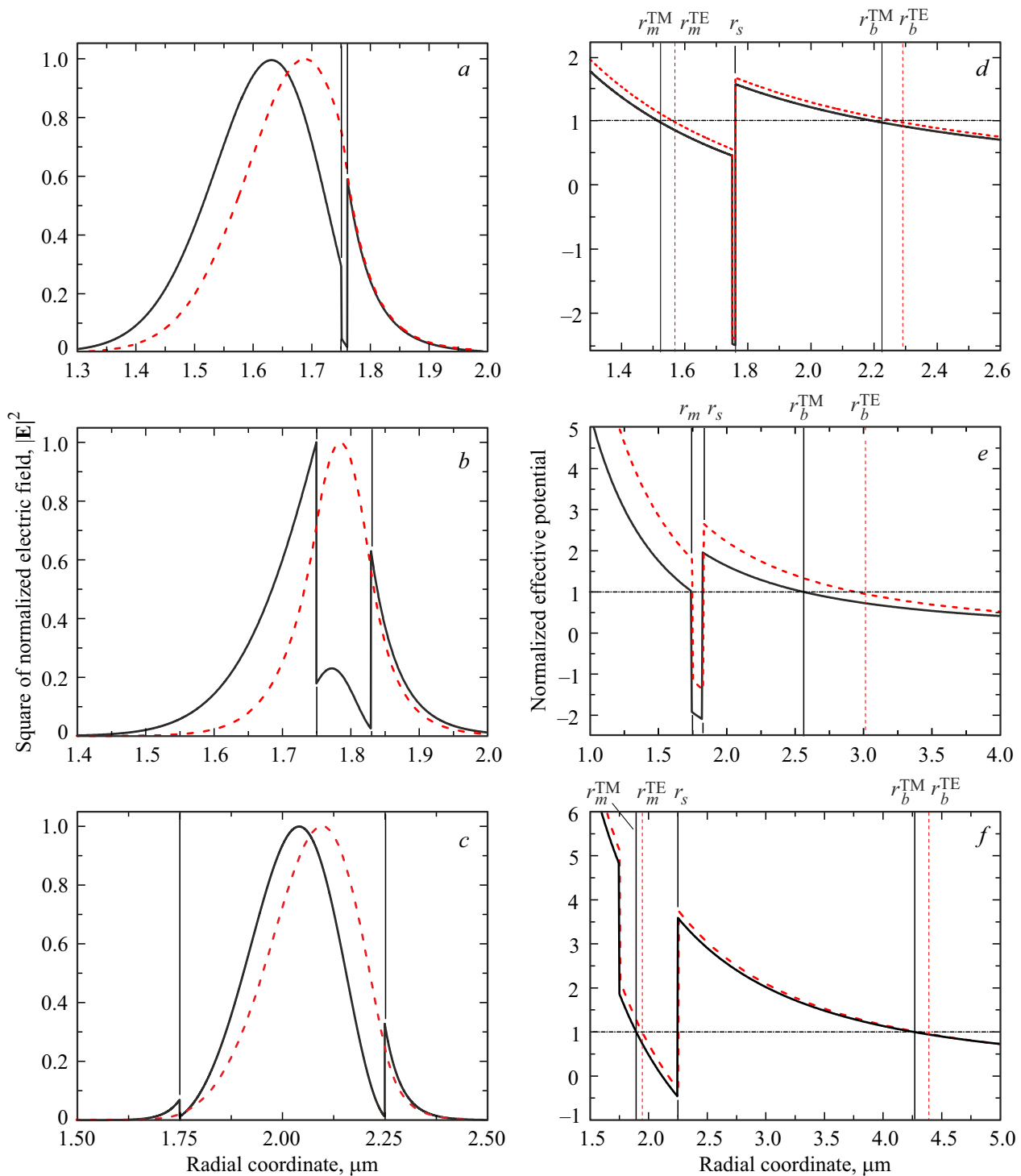


Figure 2. Distributions of squared modulus of electric field strength (*a, b, c*) and normalized effective potential (V_{ef}/E) (*d, e, f*) for whispering gallery modes TE_{32}^1 (dashed line) and TM_{32}^1 (solid line) over the radial coordinate for different shell thicknesses. MR parameters and notations in the figure are described in the text.

boundary playing an important role in forming the mode. Maxima of both modes are located inside the shell. With this thickness the level of energy for both modes is in the potential well formed by the step changes of potential at the shell boundaries (Fig. 2, *e*). Points of turn coincide with

these boundaries. Thus, both modes propagate as waveguide modes inside the shell, that plays a role of waveguide, at the same time they undergo multiple reflections from both its boundaries. Due to the reflection from the shell/core boundary an additional phase difference arises between TE-

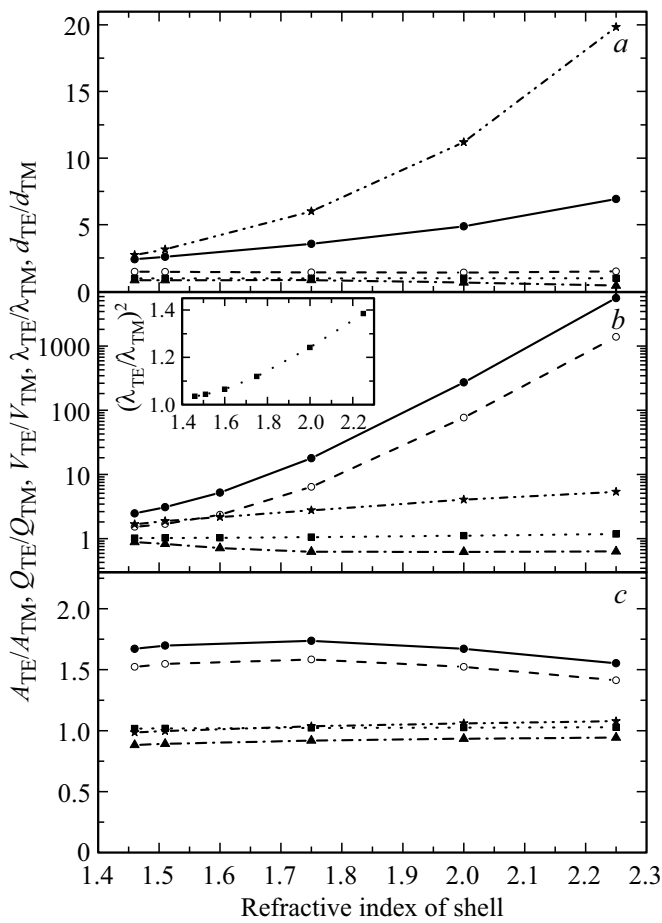


Figure 3. Dependence of peak amplitude ratio (A_{TE}/A_{TM} — solid line), Q-factors (Q_{TE}/Q_{TM} — dashed line), wavelengths ($\lambda_{TE}/\lambda_{TM}$ — dotted line), effective mode volumes (V_{TE}/V_{TM} — dash-dotted line) and d_{TE}/d_{TM} — das-dotted - dotted line for TE_{32}^1 and TM_{32}^1 modes on the refractive index of the shell. Shell thickness: 10 (a), 80 (b), and 500 nm (c). The insert shows graph $(\lambda_{TE}/\lambda_{TM})^2$ in the linear scale for a thickness of 80 nm.

and TM- modes and, as a consequence, the difference between wavelengths of modes increases. This results in that height and width of the potential barrier for the TE-mode are significantly (by 1.79 and 1.62 times) exceed height and width for the TM-mode (Fig. 2, e). This, in turn, leads to a multifold decrease in the probability of tunneling through the potential barrier for the TE-mode as compared with the TM-mode and, respectively, multifold growth of Q-factor for the TE-mode as compared with the TM-mode (Fig. 3, b).

The rate of spontaneous emission in the WGM inside the spherical microresonator Γ_{cav} as compared with the case of radiation in free space Γ_{free} increases due to the Purcell effect [27] by the following factor:

$$\frac{\Gamma_{cav}}{\Gamma_{free}} = \frac{3Q(\lambda/n)^3}{4\pi^2 V_{ef}} \frac{|\mathbf{dE}(\mathbf{r}_e)|^2}{|\mathbf{d}|^2},$$

where Q — Q-factor of the mode, V_{ef} — effective mode volume, λ — wavelength of the mode in vacuum, n —

refractive index, \mathbf{d} — transition dipole moment, $\mathbf{E}(\mathbf{r}_e)$ — electric field of the mode, that is normalized so that in the maximum it is equal to 1, \mathbf{r}_e — position of the radiator inside the resonator [28]. Respectively, the peak amplitude in the radiation spectrum of the shell is proportional to the rate of spontaneous emission. The ratio of peak amplitudes A_{TE}/A_{TM} will be contributed by ratios of all parameters in this formula, namely Q-factors of these modes Q_{TE}/Q_{TM} , effective mode volume V_{TE}/V_{TM} , wavelengths $\lambda_{TE}/\lambda_{TM}$ and integrals:

$$d_{TE}/d_{TM} = \int |\mathbf{dE}_{TE}(\mathbf{r})|^2 dV / \int |\mathbf{dE}_{TM}(\mathbf{r})|^2 dV$$

(the integration is over the total volume of the shell).

For the three above-mentioned thicknesses of the shell we have investigated the dependence of peak amplitudes ratio (A_{TE}/A_{TM}), Q-factors ratio (Q_{TE}/Q_{TM}), wavelengths ratio ($\lambda_{TE}/\lambda_{TM}$), effective volumes ratio (V_{TE}/V_{TM}) and d_{TE}/d_{TM} for TE_{32}^1 and TM_{32}^1 modes on the refractive index of the shell (Fig. 3).

With a thickness of 500 nm all the ratios: Q_{TE}/Q_{TM} , $\lambda_{TE}/\lambda_{TM}$, V_{TE}/V_{TM} , and d_{TE}/d_{TM} are weakly dependent on the refractive index of the shell (Fig. 3, c). Wavelengths of both modes are different from each other by 2–3%, potential barriers differ insignificantly (Fig. 2, f) and, as a consequence, Q-factors differ by approximately 1.5 times. Radial distribution profiles of fields of both modes are almost completely inside the radiating shell (Fig. 2, c), therefore the ratio of d_{TE}/d_{TM} is close to one as well. As a result the ratio of A_{TE}/A_{TM} changes insignificantly depending on the refractive index of the shell and has a low absolute value (1.4–1.74).

With a thickness of 10 nm (Fig. 3, a) in the investigated range of the shell refractive index the ratios of Q-factors Q_{TE}/Q_{TM} , wavelengths $\lambda_{TE}/\lambda_{TM}$, and effective volumes V_{TE}/V_{TM} change insignificantly. However, d_{TE}/d_{TM} and A_{TE}/A_{TM} increase monotonously. Due to the presence of the dip in the field profile, the electric field of the TM-mode decreases in the region of shell, where radiating centers are located, in relation to the electric field of the TE-mode (Fig. 2, a). Depth of the dip is defined by the magnitude of the electric field radial component step at the interface between two media, which is equal to the ratio of dielectric permittivity values of these media ($E_1/E_2 = \varepsilon_2/\varepsilon_1$, where E_1, E_2 — radial components of the electric field at the interface between two media with dielectric permittivity values of $\varepsilon_1, \varepsilon_2$, respectively) [29]. Depth of the dip increases as increases the ratio of dielectric permittivity of the shell to the dielectric permittivity of the environment and the core. This explains the increase in d_{TE}/d_{TM} with growth of the refractive index of the shell and, as a consequence, the increase in the A_{TE}/A_{TM} peak amplitude ratio (Fig. 3, a). The difference between d_{TE}/d_{TM} and A_{TE}/A_{TM} is connected with the approximate procedure of the d_{TE}/d_{TM} calculation.

With a thickness of 80 nm (Fig. 3, b) the ratio of wavelengths $\lambda_{TE}/\lambda_{TM}$ and effective volumes V_{TE}/V_{TM} in

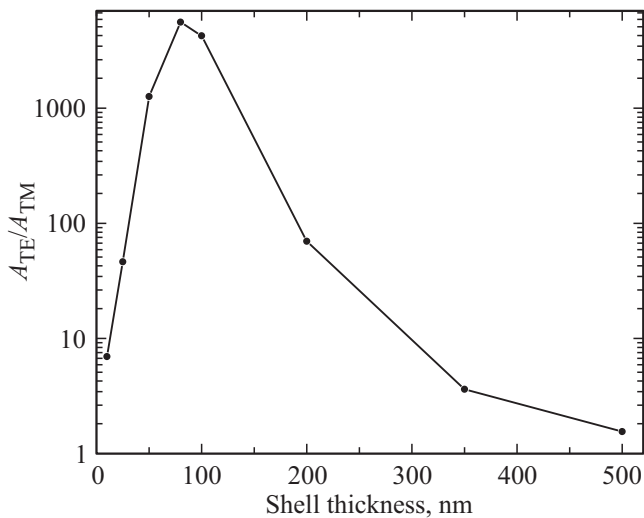


Figure 4. Dependence of A_{TE}/A_{TM} peak amplitude ratio for TE_{32}^1 and TM_{32}^1 modes on the shell thickness. Refractive index of the shell 2.25.

the range of shell refractive index in question change insignificantly. Due to the increase in depth of the dip in the field profile (Fig. 2, *b*), the ratio of d_{TE}/d_{TM} increases by 3.2 times. However, a considerably different behavior is observed for the A_{TE}/A_{TM} and Q_{TE}/Q_{TM} dependencies as compared with the cases of thin (Fig. 3, *a*) and thick (Fig. 3, *c*) shells. In the region of $n_s > 1.75$ the amplitude ratio A_{TE}/A_{TM} increases considerably with an increase in the refractive index of the shell. In the same region the ratio of Q-factors Q_{TE}/Q_{TM} also is strongly dependent on the refractive index. Thus, in the case when the refractive index of the shell is greater than the refractive index of the core, the radiation in WGM with prevailing TE-polarization can be obtained. In the considered range of n_s values the ratio of squared wavelengths $(\lambda_{TE}/\lambda_{TM})^2$ increases by 34% (the insert in Fig. 3, *b*), which results in a significant increase in height and width of the potential barrier for the TE-mode as compared with the barrier for the TM-mode (Fig. 2, *e*). Hence, the Q-factor of the TE-mode increases by several orders of magnitude as compared with the TM-mode, and increases the ratio A_{TE}/A_{TM} of peak amplitudes. The dip of field profile in the shell region for the TM-mode as compared with the TE-mode (Fig. 2, *b*) also contributes to the increase of A_{TE}/A_{TM} , but it is not a definitive factor.

Fig. 4 shows the calculated dependence of A_{TE}/A_{TM} peak amplitude ratio for TE_{32}^1 and TM_{32}^1 modes on the thickness of the shell with a refractive index of $n_s = 2.25$. In the region of 10–80 nm A_{TE}/A_{TM} increases rapidly with increase in thickness; in the region higher than 100 nm a gradual decrease in A_{TE}/A_{TM} takes place. Maximum value of A_{TE}/A_{TM} is achieved at a shell thickness of 80 nm, which is optimum to amplify peaks of TE-modes as compared with TM-modes at the given refractive index of the shell. With this thickness a waveguide mode of wave mode propagation in the shell is implemented.

Thus, if the refractive index of the shell is greater than the refractive index of the core, then at a certain subwavelength thickness of the shell the amplitude of the TE mode emission peak can be significantly greater than the amplitude of the TM mode peak. Due to this the number of detected lines in experimental spectra will be reduced, which allows avoiding the high density of the frequency spectrum of eigenmodes. Such structures can be manufactured by applying a luminescent shell with a greater refractive index (for example, SiC [15]) on a core made of optically transparent SiO_2 [30] or applying a porous SiO_2 -shell [17–19] with subsequent filling of pores with radiating materials with high refractive index.

In the considered model of ideal MR there is only one mechanism of WGM broadening connected with radiation loss caused by the wave output beyond the microsphere boundary, and this mechanism defines the calculated (radiation) Q-factor (Fig. 3). In real MRs there are several other possible mechanisms that cause additional WGM broadening. Among these mechanisms are the scattering of electromagnetic wave on surface roughness, scattering on irregularities of MR substance density, absorption in the MR core and shell, inhomogeneous broadening due to MR nonsphericity, uniform and related to the wave leakage into the substrate, on which the MR is placed. These mechanisms may increase in different ways the width of modes with different Q-factors and different polarization, which will have an effect on the A_{TE}/A_{TM} peak amplitude ratio.

Conclusion

In this study we have considered the polarization effects in radiation spectra of core–shell MRs, where a luminescent shell with a refractive index greater than that of the core is applied on a spherical optically transparent small-diameter ($3.5\ \mu\text{m}$) dielectric core. The luminescence spectra of the shell, the radial distribution of the WGM electric field, wavelength, Q-factor, and effective volume of WGM are calculated using the method of electromagnetic wave field expansion in the basis of vector spherical harmonics and the method of spherical wave transfer matrices. The luminescence spectrum is composed of a large number of ordered pairs of peaks corresponding to TE- and TM-polarized WGMs.

We have investigated the dependence of (A_{TE}/A_{TM}) peak amplitude ratio for TE_{32}^1 and TM_{32}^1 modes on the refractive index and thickness of the shell.

It is shown that when the optical thickness of the shell is much less than the wavelength of modes, the WGM field is predominantly localized in the core. With a small shell thickness (10 nm) the A_{TE}/A_{TM} ratio increases monotonously with increase in the refractive index of the shell, and peak amplitude of the TE-mode can be several times higher than peak amplitude of the TM-mode.

With a large shell thickness (500 nm) the WGM field is almost completely localized in the shell. At the same time peak amplitudes differ insignificantly (approximately by ~ 1.7 times), and their ratio is weakly dependent on the refractive index of the shell.

At certain intermediate shell thicknesses (80 nm), when optical thickness of the shell is several times less than wavelengths of the modes in question, field of both modes is localized in both the shell and in the core. At the same time the ratio of peak amplitudes, A_{TE}/A_{TM} , increases exponentially with increase in the refractive index of the shell and can be as high as several orders of magnitude. This is explained by the fact that WGMs propagate inside the shell as waveguide modes. Thus, by selecting parameters of the shell, it is possible to achieve the situation when the radiation leaves the MR predominantly in the form of TE-polarized WGMs.

Funding

The study was carried out using state budget funds on the topic of state assignment 0040-2019-0012.

Conflict of interest

The authors declare that they have no conflict of interest.

References

- [1] M.R. Foreman, J.D. Swaim, F. Vollmer. *Adv. Opt. Photon.*, **7** (2), 168 (2015). DOI: 10.1364/AOP.7.000168
- [2] J. Ward, O. Benson. *Las. Photon. Rev.*, **5** (4), 553 (2011). DOI: 10.1002/lpor.201000025
- [3] A. Chiasera, Y. Dumeige, P. Féron, M. Ferrari, Y. Jestin, G. Nunzi Conti, S. Pelli, S. Soria, G.C. Righini. *Las. Photon. Rev.*, **4** (3), 457 (2010). DOI: 10.1002/lpor.200910016
- [4] Y.P. Rakovich, J.F. Donegan. *Las. Photon. Rev.*, **4** (2), 179 (2010). DOI: 10.1002/lpor.200910001
- [5] G.C. Righini, S. Soria. *Sensors*, **16** (6), 905 (2016). DOI: 10.3390/s16060905
- [6] L. Cai, J. Pan, Y. Zhao, J. Wang, S. Xiao. *Phys. Status Solidi A*, **217** (6), 1900825 (2020). DOI: 10.1002/pssa.201900825
- [7] D. Venkatakrishnarao, E.A. Mamonov, T.V. Murzina, R. Chandrasekar. *Adv. Opt. Mater.*, **6**, 1800343 (2018). DOI: 10.1002/adom.201800343
- [8] T. Reynolds, N. Riesen, A. Meldrum, X. Fan, J.M.M. Hall, T.M. Monro, A. François. *Las. Photon. Rev.*, **11** (2), 1600265 (2017). DOI: 10.1002/lpor.201600265
- [9] F. Vollmer, S. Arnold. *Nat. Methods*, **5** (7), 591 (2008). DOI: 10.1038/NMETH.1221
- [10] X. Jiang, A.J. Qavi, S.H. Huang, L. Yang. *Matter*, **3** (2), 371 (2020). DOI: 10.1016/J.MATT.2020.07.008
- [11] Y. Zhi, X.-C. Yu, Q. Gong, L. Yang, Y.-F. Xiao. *Adv. Mater.*, **29** (12), 1604920 (2017). DOI: 10.1002/adma.201604920
- [12] I. Teraoka, S. Arnold. *J. Opt. Soc. Am. B*, **23** (7), 1434 (2006). DOI: 10.1364/JOSAB.23.001434
- [13] I. Teraoka, S. Arnold. *J. Opt. Soc. Am. B*, **24** (3), 653 (2007). DOI: 10.1364/JOSAB.24.000653
- [14] D. Ristić, A. Chiappini, M. Mazzola, D. Farnesi, G. Nunzi Conti, G.C. Righini, P. Féron, G. Cibiel, M. Ferrari, M. Ivanda. *Eur. Phys. J. Special Topics*, **223** (10), 1959 (2014). DOI: 10.1140/epjst/e2014-02239-2
- [15] S.A. Grudinkin, A.A. Dontsov, N.A. Feoktistov, M.A. Baranov, K.V. Bogdanov, N.S. Averkiev, V.G. Golubev. *Semiconductors*, **49** (10), 1369 (2015). DOI: 10.1134/S1063782615100085.
- [16] D. Ristic, A. Chiappini, A. Chiasera, C. Armellini, A. Carpentiero, M. Mazzola, E. Moser, S. Varas, S. Berneschi, G. Nunzi Conti, S. Pelli, S. Soria, G. Speranza, L. Lunelli, C. Pederzoli, F. Prudenzano, P. Feron, M. Ivanda, G. Cibiel, G.C. Righini, M. Ferrari. In: *Laser Resonators, Microresonators, and Beam Control XIV*, ed. by A.V. Kudryashov, A.H. Paxton, V.S. Ilchenko. *Proc. SPIE*, **8236**, 82361W (2012). DOI: 10.1117/12.910104
- [17] E.Yu. Trofimova, D.A. Kurdyukov, S.A. Yakovlev, D.A. Kirilenko, Yu.A. Kukushkina, A.V. Nashchekin, A.A. Sitnikova, M.A. Yagovkin, V.G. Golubev. *Nanotechnol.*, **24** (15), 155601 (2013). DOI: 10.1088/0957-4484/24/15/155601
- [18] D.A. Kurdyukov, D.A. Eurov, D.A. Kirilenko, J.A. Kukushkina, V.V. Sokolov, M.A. Yagovkina, V.G. Golubev. *Micro. Mesopor. Mater.*, **223**, 225 (2016). DOI: 10.1016/j.micromeso.2015.11.018
- [19] D.A. Kurdyukov, D.A. Eurov, D.A. Kirilenko, V.V. Sokolov, V.G. Golubev. *Micro. Mesopor. Mater.*, **258**, 205 (2018). DOI: 10.1016/j.micromeso.2017.09.017
- [20] A. Weller, F.C. Liu, R. Dahint, M. Himmelhaus. *Appl. Phys. B*, **90** (3), 561 (2008). DOI: 10.1007/s00340-007-2893-2
- [21] M. Himmelhaus, S. Krishnamoorthy, A. Francois. *Sensors*, **10** (6), 6257 (2010). DOI: 10.3390/s100606257
- [22] M.A. Kaliteevski, S. Brand, R.A. Abram, V.V. Nikolaev. *J. Modern Optics*, **48** (9), 1503 (2001). DOI: 10.1080/09500340108231779
- [23] *Glass Micro- and Nanospheres Physics and Applications*, ed. by G.C. Righini (Jenny Stanford Publishing, New York, 2019). DOI: 10.1201/b22474
- [24] J.M.M. Hall, T. Reynolds, M.R. Henderson, N. Riesen, T.M. Monro, S. Afshar. *Opt. Expr.*, **25** (6), 6192 (2017). DOI: 10.1364/OE.25.006192
- [25] A.A. Dukin, V.G. Golubev. *Opt. i spektr.*, **129** (10), 1314 (2021) (in Russian). DOI: 10.21883/OS.2021.10.51499.2266-21
- [26] M.L. Gorodetsky, *Opticheskie mikrorezonatory s gigantskoj dobrotnost'yu* (Fizmatlit, Moskva, 2011) (in Russian).
- [27] E.M. Purcell. *Phys. Rev.*, **69** (11–12), 681 (1946). DOI: 10.1103/physrev.69.674
- [28] *Confined Photon Systems: Fundamentals and Applications*, ed. by H. Benisty, C. Weisbuch, J.-M. Gérard, R. Houdré, J. Rarity (Springer-Verlag, Berlin Heidelberg, 1999).
- [29] J.R. Reitz, F.J. Milford, R.W. Christy. *Foundations of Electromagnetic Theory*, 4th ed. (Addison-Wesley, 2008).
- [30] E.Y. Trofimova, A.E. Aleksenskii, S.A. Grudinkin, I.V. Korokin, D.A. Kurdyukov, V.G. Golubev. *Colloid J.*, **73** (4), 546 (2011). DOI: 10.1134/S1061933X11040156